

Deprotonation of Solvated Formic Acid: Car–Parrinello and Metadynamics Simulations

Jung-Goo Lee,[†] Eliana Asciutto,[†] Volodymyr Babin,[†] Celeste Sagui,[†] Thomas Darden,[‡] and Christopher Roland^{*,†}

Center for High Performance Simulations (CHiPS) and Department of Physics, North Carolina State University, Raleigh, North Carolina 27695 and the Laboratory for Structural Biology, National Institute of Environmental and Health Sciences (NIEHS), Research Triangle Park, North Carolina 27709

Received: October 11, 2005; In Final Form: December 9, 2005

The deprotonation of solvated formic acid was investigated theoretically with *ab initio* simulations. With the Car–Parrinello method, deprotonation and reprotonation by means of a proton wire were observed. The microscopies of these reactions were analyzed, and reveal the key role played by nearby water molecules in catalyzing the reactions. A constrained molecular dynamics calculation was carried out to estimate the dissociation free energy. Deprotonation of formic acid was further investigated with the recently developed metadynamics method using the formic acid oxygen coordination numbers as the collective variables. The determined free-energy landscape gives barriers similar to that obtained with the constrained free-energy calculation.

I. Introduction

Acid formation is one of the most fundamental of all chemical reactions, playing a key role in large numbers of chemical and biological processes.¹ Acidity involves the deprotonation of a chemical species in an aqueous environment. The key feature of such reactions is the interplay between the acid and the surrounding waters. While there has been a number of theoretical investigations^{2–11} of this issue, the interaction between different acids and waters has not been fully explored. Here, we report on density functional theory (DFT) simulations of the solvation and subsequent deprotonation of formic acid, the simplest carboxylic acid. Formic acid is important in a variety of industrial, food, and biological settings. It has a pK_a of 3.75, and, therefore, chemically represents an important example of an acid of intermediate strength.¹²

A key issue in any deprotonation reaction is how the solvating water molecules arrange themselves—both spatially and dynamically—thereby setting up either complex solvation shells and/or clathrate-type structures. Experimentally, this field has benefited tremendously from the development of fast spectroscopic techniques, which have enabled scientists to directly probe the dynamics and relaxation of molecules on the femto-second time scale. Similarly, X-ray and neutron diffraction studies have been invaluable in probing the hydration structures.^{13,14}

There have been classical and quantum molecular dynamics (MD) investigations complementing the experimental investigations. The advantage of such simulations is that they provide direct microscopic or atomistic information about the chemical process under study. In particular, the past few years have seen an increase in the application of Car–Parrinello¹⁵ DFT-based MD studies to this problem of solvated ions and molecules. With Car–Parrinello MD, it is possible to describe all the details of bond-formation, bond-breakage, and the associated dynamics

in a self-consistent fashion subject to the limitations of the adiabatic propagation of the nuclear degrees of freedom. As a technique, it is, therefore, considered to be significantly more reliable than the potential-based classical MD methods, which often have great difficulty describing molecular dissociation correctly. The insights gained are then often used as the guide for more accurate modeling based on quantum chemistry methods.

Unfortunately, Car–Parrinello and other DFT-based simulations tend to be computationally quite expensive, so that current investigations are typically limited to tens of water molecules over a tens of picosecond time scale. Such a short period of time is typically not enough to probe many chemical reactions of interest, because even systems with a modest activation barrier require very long simulation times. An alternative approach to this problem is given by the recently developed metadynamics method.^{16–18} This method is based on extended Lagrangian and coarse-grained non-Markovian dynamics, and is presently being applied to an ever growing number of chemical reactions.^{16,17,19–25} A key feature is that it allows for systems to take different, more efficient pathways in its exploration of a complex free-energy surface and thereby investigate the rare events of a system. Metadynamics simulations can, therefore, be used to explore chemical reactions involving several energy barriers in a relatively short period of time.

Here, we report on an extensive theoretical investigation of formic acid deprotonation by means of Car–Parrinello and metadynamics simulations. Formic acid de- and re-protonation events were observed with the Car–Parrinello-based DFT simulations. The configurations and microscopies of these events were then analyzed with a focus on the role of the surrounding waters in initiating the proton transfer. A constrained molecular dynamics simulation was then used to estimate the dissociation free energy. As a complement to these studies, we investigated formic acid deprotonation with the metadynamics methods using both one and two collective variables. Each of these simulation methods provides us with a different estimate of the free-energy

* Corresponding author. E-mail: roland@gatubela.physics.ncsu.edu.

[†] North Carolina State University.

[‡] National Institute of Environmental and Health Sciences.

difference, as they sample different distribution functions, paths through phase space, etc. It is, however, reassuring that the resulting estimates of the dissociation free energies are in reasonable agreement with those obtained by means of the constrained MD simulations.

II. Computational Methodology

A. Car–Parrinello Molecular Dynamics Simulations. We have used the standard Car–Parrinello¹⁵ DFT-based ab initio MD method to investigate the solvated acid. Such an approach has already been used to study dissociation of other acids such as HCl, HBr, and HF.^{2–5} The approach is able to correctly describe both bond-breakage and bond-formation, all in a self-consistent manner. The *initial* simulations were carried out in the microcanonical ensemble with the popular CPMD²⁶ code. The system consisted of 63 water molecules from a previously equilibrated bulk water simulation, plus the acid molecule all in a cubic box of 12.517 Å subject to periodic boundary conditions. The simulations were carried with the Vanderbilt ultra-soft pseudopotentials²⁷ with a cutoff of 25 Ry and with the Perdew–Burke–Ernzerhof (PBE)^{28,29} functional and a fictitious electron mass of 900 au.^{30–32} For the formic acid molecule, the initial torsional angle of the HC–OH bond was taken to be 180°, i.e., the molecule was started in the trans conformation. The temperature of the system was slowly raised from zero to 300 °K, and then equilibrated for over 1.0 ps. Phase space trajectories were then collected for over 18 ps, with a small time step of 0.0363 fs.

Generally speaking, the dissociation process of an acid is a rare event that is difficult to observe over the time span of a short DFT-based simulations. To quantify the dissociation of formic acid (i.e., $\text{HCOOH} + \text{H}_2\text{O} \rightarrow \text{HCOO}^- + \text{H}_3\text{O}^+$), we calculated free energies using both constrained molecular dynamics^{7,8,32} and metadynamics simulations.^{16,17} In terms of the former, one selects a constraint ξ (typically a distance), whose value is varied between two limits in suitable intervals. For each interval, trajectories are collected and the force of constraint measured. From such simulations, the relative free energies between states ξ_i and ξ_f may be obtained from the following expressions:

$$\Delta F = - \int_{\xi_i}^{\xi_f} f_{\xi} d\xi' \quad (2.1)$$

where

$$f_{\xi} = \frac{\langle Z^{-1/2} [\lambda - k_B T G] \rangle_{\xi}}{\langle Z^{-1/2} \rangle_{\xi}} \quad (2.2)$$

Here, f_{ξ} is the average force of constraint, k_B the Boltzmann constant, T the temperature, and Z and G are weight and correction factors, respectively. It can be shown, that in the case of a simple distance constraints, these equations reduce to the ensemble average of the Lagrange multiplier λ , and $f_{\xi} = \langle \lambda \rangle_{\xi}$. A straightforward thermodynamic integration then gives the free-energy profile. This approach is now relatively standard, and has previously been used to calculate dissociation free energies.^{6,9}

B. Metadynamics Method. We have investigated the deprotonation of formic acid by means of metadynamics simulations, as an alternate to the method of constrained dynamics. The advantage of this approach is that the metadynamics method allows for a relatively quick and efficient sampling of the

configuration space, which is something that is difficult to achieve in a regular MD simulation. Details of the metadynamics method have already been extensively published,^{16–18} and will, therefore, be only briefly reviewed here. The initial crucial step in any metadynamics simulation involves the identification of the *collective variables* (CV) for the problem, which are denoted by $S_a(\mathbf{R})$, $a = 1, \dots, n$ and are to be analytic functions of the ionic positions \mathbf{R} . The CVs should include all the relevant modes that are difficult to sample during a regular MD simulation, as well as being able to distinguish between reactants and products. Typical CVs include bond distances, dihedral and/or torsional angles, coordination numbers, etc. Once the CVs are chosen, the artificial *metadynamics* of the system is generated by the extended Lagrangian:

$$L = L_{CP} + \frac{1}{2} \sum_{a=1}^n [M_a \dot{s}_a^2 - k_a (S_a(\mathbf{R}) - s_a)^2] - V(t, \{s_a\}) \quad (2.3)$$

Here, L_{CP} represents the standard Car–Parrinello Lagrangian that drives the electronic and ionic dynamics.¹⁵ The CVs are coupled to an additional dynamical variables s_a by means of a harmonic potential. With these variables s_a is associated with a fictitious kinetic energy and a time-dependent potential $V(t, \{s_a\})$. This time-dependent potential is crucial. It is constructed out of repulsive inverted Gaussians, it drives the system out of any free-energy minima, and forces it to explore as of yet unexplored regions of the configuration space. For the vectors $\mathbf{s} = \{s_a\}$ and $\mathbf{s}^i = \{s_a(t_i)\}$, $V(t, \mathbf{s})$ was chosen to have the following form:

$$V(t, \mathbf{s}) = W \sum_{t_i < t} \exp \left\{ - \frac{(\mathbf{s} - \mathbf{s}^i)^2}{2(\Delta s^{\perp})^2} \right\} \times \exp \left\{ - \frac{[(\mathbf{s}^{i+1} - \mathbf{s}^i) \cdot (\mathbf{s} - \mathbf{s}^i)]^2}{2(\Delta s^{\parallel})^4} \right\} \quad (2.4)$$

This shape of the Gaussian is adapted to the topology of the free-energy surface. In particular, Δs^{\perp} gives the size of the Gaussians in a direction perpendicular to the motion, while $\Delta s^{\parallel} = |\mathbf{s}^{i+1} - \mathbf{s}^i|$ gives the size in a direction parallel to the motion, and W is a prefactor controlling the amplitude of the individual hills. The mass M_a and coupling constant k_a determine the rate of time evolution of the metadynamics with respect to the otherwise standard electronic and ionic degrees of freedom. Essentially, their values are chosen such that the dynamics of the variables $\{s_a\}$ are decoupled from the other degrees of freedom, so that $V(t, \mathbf{s})$ approaches the free-energy $F(\mathbf{s})$ of the system, i.e., within a constant. The accuracy of the free-energy

$$V(t, \mathbf{s})_{t \rightarrow \infty} = -F(\mathbf{s}) \quad (2.5)$$

profile, determined by the metadynamics simulation, depends on the size of the time-dependent inverted Gaussians. For low rates of accumulation and small-amplitude Gaussians, the determination of $F(\mathbf{s})$ should indeed be quite accurate.

III. Results and Discussion

A. Car–Parrinello MD Simulations. The following is a summary of the salient features of the deprotonation of solvated formic acid, as shown in Figure 1. During the first 0.38 ps, the

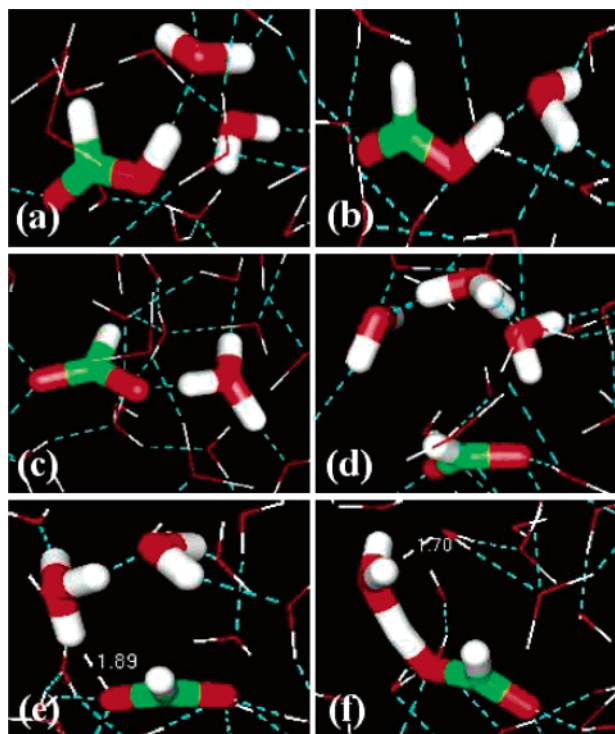


Figure 1. Details from the Car–Parrinello simulation showing the deprotonation (a–c), and subsequent reprotonation (d–f) events for solvated formic acid. Specific times are: (a) 0.39 ps; (b) 3.38 ps; (c) 4.68 ps; (d) 5.14 ps; (e) 5.31 ps; (f) 5.37 ps, respectively. Only the most relevant molecules are shown and highlighted. Dashed lines indicate the hydrogen bonds.

HC–OH bond rotated from its initial trans to a cis form. During this time, the hydroxyl moiety of the formic acid (left molecule) formed a hydrogen bond with an incoming water molecule (top water in Figure 1a), while the water that formed a hydrogen bond with the formic acid in its initial trans-state (right molecule) begins to move away. At time $t = 3.88$ ps (Figure 1b), the distance between the O-atom on the now hydrogen-bonded water, and the H-atom on the formic acid became a close 1.34 Å, as compared to the more usual hydrogen bond length of ~ 1.8 Å. At about 4.68 ps (Figure 1c), the deprotonation of the formic acid was first observed to take place, with the formation of the HCOO^- and $(\text{H}_3\text{O})^+$ species. For a fraction of a picosecond, the proton appeared to jump back and forth between the two species.

At this stage, the formic acid has de facto lost its proton, and formed the anion. It is interesting to note, that aside from the deprotonation, we also observed the subsequent reprotonation of the formate anion via a proton channel, which in this case involves a “ring” of three water molecules shown in Figures 1d–1f. During much of this time, the anion and hydronium cation formed a solvent-separated pair, with at least one or more waters separating the two. The multistep reprotonation process was completed at $t = 5.37$ ps. No additional events were observed until about 14.71 ps, when the acid began to deprotonate once more, with the proton moving back and forth between the formic acid and the water molecules. Ultimately, even though a proton-transfer event was observed, a fluctuation ended up bringing the transferred proton back toward the formate anion, which was then reprotonated once more.

To gain further insight into the proton transfer event, we have explicitly analyzed the motions of all the water molecules in the system. The simulations suggest that the proton transfers are mediated by the presence of additional water molecules,

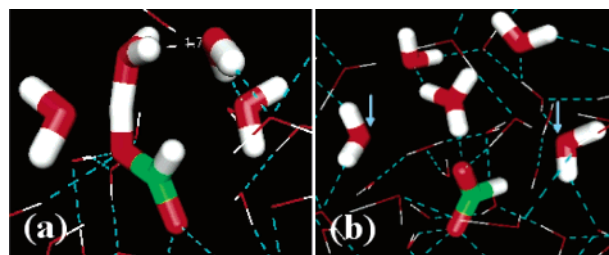


Figure 2. Snapshots and details from the Car–Parrinello simulation of formic acid showing more details of two proton-transfer events: (a) the proton wire that reprotonates the formic anion at 5.37 ps; (b) deprotonation events at 14.71 ps. Important second-shell waters that appear to catalyze the proton-transfer events are marked with arrows.

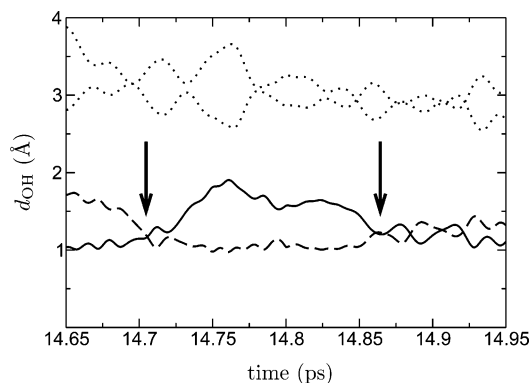


Figure 3. Fluctuations in d_{OH} as a function of time for the $t = 14.71$ ps proton-transfer event. Here, the solid line represents d_{OH} for the formic acid; dashed line, d_{OH} for the primary water forming the hydronium ion; and dotted line, the second-shell waters. Arrows mark the proton-transfer events.

located primarily beyond the first solvation shell, as shown in Figure 2. Figure 2a presents a more detailed version of Figure 1f, showing details of the reprotonation process. Toward the right are the three water molecules that form the proton wire, which is responsible for channeling the proton from one end of the formic acid molecule to the other. Toward the left, we observe the presence of an additional water molecule, that appears to mediate the reprotonation of the formate anion. The presence of such additional waters are familiar from other studies of proton transfer in bulk waters, and, as we will discuss, play a key role in the proton-transfer events between the acid and water molecules. For instance, Figure 2b shows a snapshot of a later time configuration ($t = 14.71$ ps), as the formic acid molecule deprotonates once more. Again, note the presence of now two water molecules (marked by arrows) out in the second solvation shell, which are oriented as the leftmost water in Figure 2a. Also note that the primary water molecule (which receives the proton) is hydrogen bonded with other waters reaching into the bulk. These waters, form a “V-shape” $(\text{H}_7\text{O}_3)^+$ cluster, similar to the Zundel complexes observed in other ab initio simulations of bulk water.³³

To quantify the motion of the nearby waters, we have plotted in Figure 3 the typical O–H distance (d_{OH}) as a function of time, with H representing the proton that is currently active and undergoing exchange. Note that the O–H distance, where O is the oxygen on the formic acid molecule (solid line), initially fluctuates ~ 1.0 Å, until the proton is transferred to the primary water. The distance then increases until a fluctuation brings the proton back to the formic acid (both events marked by an arrow). As expected, the O–H distance, now between the primary water which receives the proton (dashed line) shows the opposite behavior. Figure 3 also marks the presence of the two additional

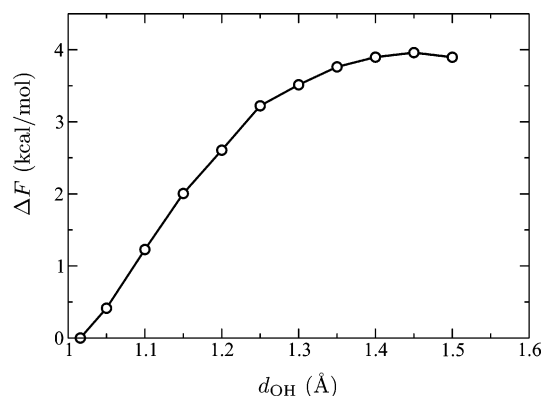


Figure 4. Free-energy profile (kcal/mol) as a function of the constrained distance for solvated formic acid.

water molecules out in the second solvation shell; these maintain a steady distance of ~ 2.6 – 3.3 Å away from the proton during the exchanges.

While we were fortunate enough to observe formic acid dissociation during the course of these short ab initio simulations, this must be considered fortuitous, since deprotonation is generally a rare event. To quantify the dissociation free energy, we first used constrained MD simulations.^{7,8} Here the constrained variable was taken to be the formic acid oxygen–hydrogen distance (i.e., $\xi = |r_O - r_H|$), which was varied between 1.00 and 1.5 Å, in increments of 0.05 Å. For each distance interval, constrained trajectories were obtained from well equilibrated, unconstrained configurations. The properties were then averaged over 3 ps—which is competitive with other constrained molecular dynamics simulations⁶—so that reasonable running averages of the constraint force were obtained. In these simulations, a constant temperature of $T = 300$ °K was maintained by means of a Nose–Hoover thermostat.³⁴ Thermodynamic integration then yielded the free-energy profile shown in Figure 4. For the constrained dynamics, the transition state turned out to be $\xi = 1.45$ Å, with a dissociation barrier of 4.0 kcal/mol. This calculated barrier (which is based on the free-energy difference) is somewhat lower than the experimental estimate of 5.1 kcal/mol as obtained from the $pK_a = 3.75$ value. This result is, however, consistent with other DFT-based simulations of other acids which also consistently obtain barriers that are lower than the experimental numbers.^{9,35,36} Here, we also note that we observed that the formate anion and hydronium cation formed a solvent-separated pair many times during the constrained simulation, especially when the oxygen–hydrogen distance was greater than 1.35 Å.

From the DFT-based simulations, it is clear that the interplay between the acid molecules and the water is an important part of the dissociation process. To gain further insight into this, we have used *static* Gaussian³⁷ calculations to further test some of the general hypothesis formed with regards to the positioning of the water molecules with respect to the formic acid. The results reported here are based on optimized geometries obtaining using the 6–31G** basis set at the MP2 level. Zero-point energies (E_0) and thermal enthalpy and free-energy corrections (H_0 and F_0) for 298.15° K were also taken into account.

As a first step, we considered the internal rotation barrier between the trans-to-cis configuration of the HC–OH bond, both in the absence and presence of a single water molecule (see Figure 5a). The latter was assumed to be hydrogen-bonded to the hydroxyl hydrogen on the formic acid. The respective rotational barriers with zero-point correction (thermal correction) from the trans position are reasonably similar: $\Delta E_o = 12.9$ kcal/

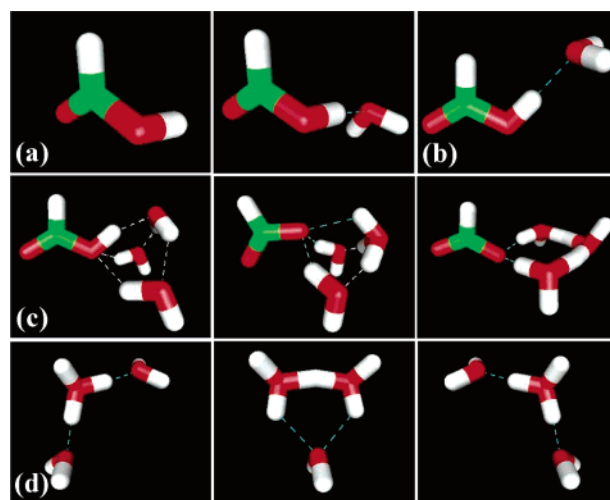


Figure 5. (a) Transition state between trans and cis formic acid with (right) and without (left) a water molecule; (b) cis formic acid hydrogen-bonded to a water molecule; (c) cis formic acid hydrogen-bonded to three water molecules (left), transition state (middle) and sample product with hydronium ion; (d) stages of proton transfer from a hydronium on to a water molecule: reactant (left), transition state (middle) and product (right).

mol ($\Delta F_o = 12.9$ kcal/mol), and $\Delta E_o = 11.1$ kcal/mol ($\Delta F_o = 10.5$ kcal/mol), respectively. The former value is close to another previous estimate of 12 kcal/mol obtained by Goddard et al.³⁸

Turning to the deprotonation reaction of formic acid, the reaction between a cis formic acid molecular and a single hydrogen bonded water molecule (Figure 5b) is quite endothermic with a very large barrier of $\Delta E_o = 190.3$ kcal/mol. This barrier is substantially reduced if two water molecules are added in positions similar to the waters marked with arrows in Figure 2b (see also Figure 5c). In this case, the saddle-point energy reduces to $\Delta E_o = 16.7$ kcal/mol ($\Delta F_o = 19.2$ kcal/mol), indicating that these waters may play a key role in catalyzing the proton transfer. This result is comparable to previous theoretical work: for example Wei et al.³⁹ computed the barrier for proton transfer from a trans formic acid molecule to a small cluster of water molecules via DFT methods. The calculated barriers without zero-point corrections were estimated to be 17.8, 16.2 (averaged), 16.6 (averaged) and 14.2 kcal/mol with one to four water molecules, respectively. In addition, Wei et al.³⁹ performed some MP2 computations on the barrier, and obtained values close to the DFT ones, differing by less than 0.7 kcal/mol. Finally, for completeness we have also investigated the proton transfer between a hydronium ion surrounded by two water molecules. Initial configuration and the transition state are shown in Figure 5d. The calculated barrier is $\Delta E_o = 5.4$ kcal/mol, which is in good agreement with previously calculated ab initio studies which find ΔE_o to range from 5.4 to 5.8 kcal/mol.^{40,41}

B. Metadynamics Simulations. Here we discuss our metadynamics runs, which represent an alternate approach to calculating the free energy of formic acid deprotonation. Essentially, metadynamics runs were carried out starting from both cis and trans configurations of the solvated formic acid with either one or two CVs. Based on previous investigations, the most natural CV associated with the problem is given by the coordination number associated with the oxygen atom on the formic acid that loses the proton. The coordination number here is simply obtained by counting the number of hydrogens less than $r_c = 1.6$ Å away from the oxygen center. To input this CV into the dynamics, it was re-expressed in the following

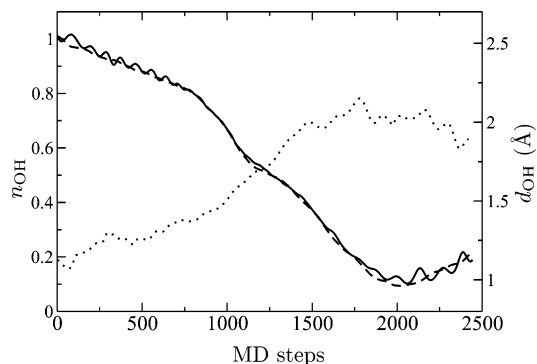


Figure 6. The time evolution of the collective variable (dashed line) and the oxygen–hydrogen coordination number (solid line) during a metadynamics run starting from the solvated cis formic acid. The dotted line shows the OH distance.

differentiable form:

$$n_{OH} = \sum_{i=1}^{N_H} \frac{1 - \left(\frac{r_{OH_i}}{r_c}\right)^6}{1 - \left(\frac{r_{OH_i}}{r_c}\right)^{18}} \quad (3.1)$$

Other parameters associated with the simulation were set as follows: the fictitious mass of the CV was selected to be 60 amu, the corresponding coupling constant was 2 au, $W = 0.13$ kcal/mol, and $\Delta s^\perp = 0.1$. New inverted Gaussians were added after at least 10 MD steps provided that the displacement of the collective variable exceeded 0.001. Otherwise, the addition was forced after 100 MD steps. We also note that the CPMD program²⁶ controls the temperature of the extra metadynamics variables by means of a velocity rescaling. Unfortunately, this leads to numerical instabilities for the metadynamics simulations with a single CV. To overcome this problem, a standard Langevin friction term⁴² was added to the CV equation of motion with a “viscosity” parameter of $\nu = 0.001$. This value turned out to be large enough to ensure numerical stability of the simulations but, at the same time, was small enough as to be negligible in comparison with the other forces acting on the collective variables.

Figure 6 shows the time evolution of the CV as obtained during a typical metadynamics run starting from the trans configuration. Note that the CV tracks the coordination number extremely well, showing that the differentiable form is reliable. It is evident that the deprotonation process begins almost immediately after the simulation is started, and is essentially completed after about 1920 MD steps. Figure 7 shows a curve of the free energy as obtained with this metadynamics run. The dissociation barrier was found to be $\Delta F \sim 4.1$ kcal/mol, which is in very good agreement with the previous results based on the constrained dynamics.

To further explore the de/re-protonation processes associated with solvated cis formic acid, the metadynamics simulations were repeated with *two* CVs. The second CV was taken to be the coordination number associated with the second oxygen of the carboxyl group of the acid. This is natural since once the proton is lost and the two oxygens are essentially equivalent. Initial exploration was conducted by means of a rather “coarse” run, with parameters $\Delta s^\perp = 0.1$, $W = 0.3$ kcal/mol and a new hill was added each 100 MD steps. In these runs, proton dissociation was observed in just 300 metadynamics steps, with

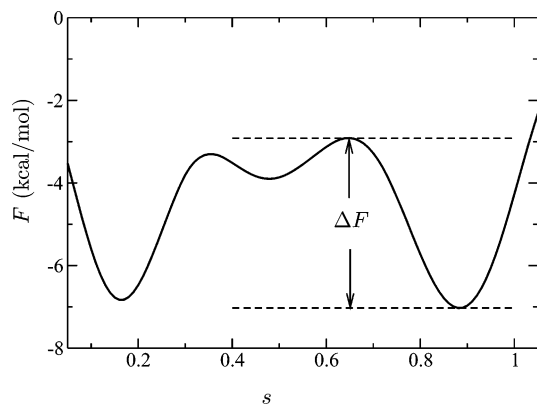


Figure 7. The one-dimensional free-energy profile as a function of the single collective variable, as obtained with the metadynamics simulation. The estimated dissociation barrier is marked. The smoothness of the curve is a result of the very large number of Gaussians added during the metadynamics run.

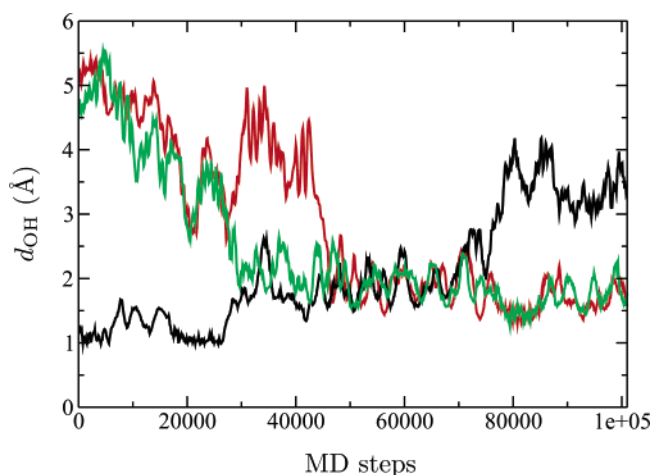


Figure 8. The oxygen–hydrogen distance obtained during a rather “fast” metadynamics run with two collective variables. Note that three hydrogens were found to be important.

a barrier of 4.7 kcal/mol. Once the dissociation was observed, reprotonation of the other oxygen atom (associated with the second CV) was observed. We note, however, that this reprotonation process did not resemble the fluctuation described in the previous section. Other configurations observed during the runs are similar to those previously described. In particular, once the deprotonation process took place (thereby forming H_3O^+), two other hydrogens from the first shell waters come in, and associate themselves with the two oxygens. These then fluctuate back and both between the acid and water molecules, as shown in Figure 8.

Figure 9 plots the time evolution of the two CVs as obtained from a more accurate simulation ($W = 0.06$ kcal/mol with inverted Gaussians added every 20 MD steps in order to accelerate the reaction). Again, dissociation was observed after about 6000 MD steps. Subsequently, the system simply fluctuates, with considerable de- and re-protonation reactions taking place at one or the other of the carboxyl oxygens. The now *two-dimensional* free-energy surface associated with these processes is shown in Figure 10. The initial (I) and deprotonated (D) states are marked, as well as the location of the saddle point (S). The calculated dissociation barrier associated with this run is ~ 3.7 kcal/mol, which is somewhat smaller than the barrier obtained for the runs with a single CV. This slightly lower barrier appears to be due to a cooperative effect, by which the two CVs act in tandem to de- and re-protonate the oxygens.

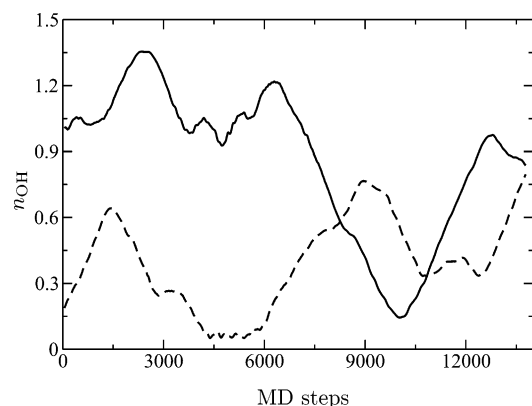


Figure 9. Time evolution of the two oxygen coordination numbers in the course of a second metadynamics simulation, for which the parameters were chosen such that the time evolution is relatively “slow”.

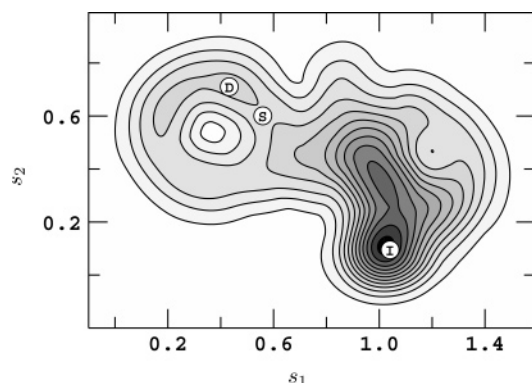


Figure 10. The contour plot of the free-energy surface as obtained with the metadynamics simulation involving two collective variables. The iso-lines are plotted 0.40 kcal/mol apart. The initial position (I), saddle point (S), and deprotonated final positions (D) for a specific trajectory, involving the deprotonation of CV s_1 are marked.

While interesting, such a dynamical effect may well be artificial and be the direct result of forcing two CVs onto the system. We note that a similar difference between the one and two CV metadynamics simulations has recently been noted in a different context.³⁶

IV. Summary

We have investigated the deprotonation the simplest carboxylic acid—formic acid—with both Car–Parrinello and metadynamics simulations. In the course of the former, formic acid was observed to deprotonate from the *cis* form, with fluctuations eventually reprotonating the anion. These processes were catalyzed by the presence of additional waters near the formic acid. Constrained molecular dynamics was used to estimate the free-energy dissociation barrier, which was found to be 4.0 kcal/mol within the context of the DFT-based simulations. Additional estimates of this barrier were obtained by means of metadynamics simulations in which versions of the oxygen (on the formic acid) coordination number were used as the collective variable. The estimates based on these metadynamics runs are of course completely different from those obtained from the constrained molecular dynamics simulation, insofar as they are based on the sampling of different distribution functions and very different paths through phase space. It is, however, reassuring that formic acid deprotonation was readily observed with these metadynamics simulations, and the estimated dissociation barrier was found to be comparable to the results obtained with the Car–Parrinello simulations.

Acknowledgment. The authors gratefully acknowledge financial support from the NSF under grants DMR-0121361 and CAREER-034039. We also thank NCSA for extensive computer support.

References and Notes

- (1) Morrison, R. J.; Boyd, R. N.; Boyd, R. K. *Organic Chemistry*, 6th edition; Benjamin-Cummings, 1992.
- (2) Laasonen, K.; Klein, M. L. *J. Am. Chem. Soc.* **1994**, *116*, 11620–11621.
- (3) Laasonen, K.; Klein, M. *J. Phys. Chem. A* **1997**, *101*, 98–102.
- (4) Kim, D.; Klein, M. *J. Am. Chem. Soc.* **1999**, *121*, 11251–11252.
- (5) Raugai, S.; Klein, M. *J. Am. Chem. Soc.* **2001**, *123*, 9484–9485.
- (6) Ivanov, I.; Klein, M. *J. Am. Chem. Soc.* **2002**, *124*, 13380–13381.
- (7) Sprik, M. *Faraday Discuss.* **1998**, *110*, 437–445.
- (8) Sprik, M. *Chem. Phys.* **2000**, *258*, 139–150.
- (9) Trout, B.; Parrinello, M. *Chem. Phys. Lett.* **1998**, *288*, 343–347.
- (10) Cuma, M.; Schmitt, U. W.; Voth, G. A. *Chem. Phys.* **2000**, *258*, 187–199.
- (11) Davies, J. E.; Doltsinis, N. L.; Kirby, A. J.; Roussev, C. D.; Sprik, M. *J. Am. Chem. Soc.* **2002**, *124*, 6594.
- (12) Patai, S. *Chemistry of Carboxylic Acids and Esters (Chemistry of Functional Groups S)*; John Wiley: 1969.
- (13) Blakeley, M.; Kalb, A.; Helliwell, J.; Myles, A. *Proc. Natl. Acad. Sci.* **2004**, *101*, 16405.
- (14) Hanson, B. *Proc. Natl. Acad. Sci.* **2004**, *101*, 16393–16394.
- (15) Car, R.; Parrinello, M. *Phys. Rev. Lett.* **1985**, *55*, 2471–2474.
- (16) Laio, A.; Parrinello, M. *Proc. Natl. Acad. Sci.* **2002**, *99*, 12562–12566.
- (17) Iannuzzi, M.; Laio, A.; Parrinello, M. *Phys. Rev. Lett.* **2003**, *90*, 238302–1.
- (18) Laio, A.; Rodriguez-Forcia, A.; Gervasio, F. L.; Ceccarelli, M.; Parrinello, M. *J. Phys. Chem. B* **2005**, *109*, 6714–6721.
- (19) Ensing, B.; Laio, A.; Gervasio, F. L.; Parrinello, M.; Klein, M. L. *J. Am. Chem. Soc.* **2004**, *126*, 9492–9493.
- (20) Churakov, S. V.; Iannuzzi, M.; Parrinello, M. *J. Phys. Chem. B* **2004**, *108*, 11567–11574.
- (21) Gervasio, F.; Laio, A.; Parrinello, M. *J. Am. Chem. Soc.* **2005**, *127*, 2600.
- (22) Ceccarelli, M.; Danelon, C.; Laio, A.; Parrinello, M. *Biophys. J.* **2004**, *87*, 58.
- (23) Iannuzzi, M.; Parrinello, M. *Phys. Rev. Lett.* **2004**, *93*, 025901.
- (24) A. Stirling, M. Iannuzzi, A. L.; Parrinello, M. *ChemPhysChem* **2004**, *5*, 1558–1568.
- (25) Asciutto, E.; Sagui, C. *J. Phys. Chem. A* **2005**, *109*, 7682–7687.
- (26) Hutter, J.; et al. *CPMD v3.9*; Copyright IBM Corp. (1990–2004) and MPI fuer Festkoerperforschung Stuttgart, 1995–2001.
- (27) Vanderbilt, D. *Phys. Rev. B* **1990**, *41*, 7892–7895.
- (28) Perdew, J.; Burke, K.; Ernzerhof, M. *Phys. Rev. Lett.* **1996**, *77*, 3865.
- (29) Perdew, J.; Burke, K.; Ernzerhof, M. *Phys. Rev. Lett.* **1997**, *78*, 1396.
- (30) Grossman, J. C.; Schwegler, E.; Draeger, E.; Gygi, F.; Galli, G. *J. Chem. Phys.* **2004**, *120*, 300.
- (31) Kuo, W.; Mundy, C. J.; McGrath, M. J.; Siepmann, J. I.; VandeVondele, J.; Sprik, M.; Hutter, J.; Chen, B.; Klein, M. L.; Mohamed, F.; Krack, M.; Parrinello, M. *J. Phys. Chem. B* **2004**, *108*, 12990.
- (32) Marwick, P.; Doltsinis, N. L.; Marx, D. *J. Chem. Phys.* **2005**, *122*, 054122.
- (33) Tuckerman, M.; Laasonen, K.; Sprik, M.; Parrinello, M. *J. Phys. Chem.* **1995**, *99*, 5749–5752.
- (34) Nose, S.; Klein, M. *Mol. Phys.* **1983**, *50*, 1055–1066.
- (35) Ensing, B.; Meijer, E.; Bloechl, P.; Baerends, E. *J. Phys. Chem. B* **2001**, *105*, 3300–3310.
- (36) Ensing, B.; Laio, A.; Parrinello, M.; Klein, M. *J. Phys. Chem. B* **2005**, *109*, 6676–6687.
- (37) Frisch, M. J.; Trucks, G. W.; Schlegel, H. B.; Scuseria, G. E.; Robb, M. A.; Cheeseman, J. R.; Montgomery, J. A., Jr.; Vreven, T.; Kudin, K. N.; Burant, J. C.; Millam, J. M.; Iyengar, S. S.; Tomasi, J.; Barone, V.; Mennucci, B.; Cossi, M.; Scalmani, G.; Rega, N.; Petersson, G. A.; Nakatsuji, H.; Hada, M.; Ehara, M.; Toyota, K.; Fukuda, R.; Hasegawa, J.; Ishida, M.; Nakajima, T.; Honda, Y.; Kitao, O.; Nakai, H.; Klene, M.; Li, X.; Knox, J. E.; Hratchian, H. P.; Cross, J. B.; Bakken, V.; Adamo, C.; Jaramillo, J.; Gomperts, R.; Stratmann, R. E.; Yazyev, O.; Austin, A. J.; Cammi, R.; Pomelli, C.; Ochterski, J. W.; Ayala, P. Y.; Morokuma, K.; Voth, G. A.; Salvador, P.; Dannenberg, J. J.; Zakrzewski, V. G.; Dapprich, S.; Daniels, A. D.; Strain, M. C.; Farkas, O.; Malick, D. K.; Rabuck, A. D.; Raghavachari, K.; Foresman, J. B.; Ortiz, J. V.; Cui, Q.; Baboul, A. G.; Clifford, S.; Cioslowski, J.; Stefanov, B. B.; Liu, G.; Liashenko, A.; Piskorz, P.; Komaromi, I.; Martin, R. L.; Fox, D. J.; Keith, T.; Al-Laham, M. A.; Peng, C. Y.; Nanayakkara, A.; Challacombe, M.; Gill, P. M. W.;

Johnson, B.; Chen, W.; Wong, M. W.; Gonzalez, C.; Pople, J. A. Gaussian 03, revision C.02; Gaussian, Inc.: Wallingford, CT, 2004.

(38) Goddard, J.; Yamaguchi, Y.; Schaefer, H., III *J. Chem. Phys.* **1992**, 96, 1158.

(39) Wei, D.; Truchon, J.; Sirois, S.; Salahub, D. *J. Chem. Phys.* **2002**, 116, 6028.

(40) Geissler, P.; Dellago, C.; Chandler, D.; Hutter, J.; Parrinello, M. *Chem. Phys. Lett.* **2000**, 321, 225–230.

(41) Geissler, P.; Voorhis, T.; Dellago, C. *Chem. Phys. Lett.* **2000**, 324, 149.

(42) Loncharich, R. J.; Brooks, B. R.; Pastor, R. W. *Biopolymers* **1992**, 32, 523–535